ACS Chemical Neuroscience

Letter

pubs.acs.org/chemneuro

The Relative Orientation of the TM3 and TM4 Domains Varies between α1 and α3 Glycine Receptors

Lu Han,[†] Sahil Talwar,[†] and Joseph W. Lynch*[,†,‡]

[†]Queensland Brain Institute and [‡]School of Biomedical Sciences, The University of Queensland, Brisbane QLD 4072, Australia

Supporting Information

ABSTRACT: Glycine receptors (GlyRs) are anion-conducting members of the pentameric ligand-gated ion channel family. We previously showed that the dramatic difference in glycine efficacies of α1 and α3 GlyRs is largely attributable to their nonconserved TM4 domains. Because mutation of individual nonconserved TM4 residues had little effect, we concluded that the efficacy difference was a distributed effect of all nonconserved TM4 residues. We therefore hypothesized that the TM4 domains of α1 and α3 GlyRs differ in structure, membrane orientation, and/or molecular dynamic properties. Here we employed voltage-clamp fluorometry to test whether their TM4 domains interact differently with their respective TM3 domains. We found a rhodamine fluorophore covalently attached to a homologous TM4 residue in each receptor interacts differentially with a conserved TM3 residue. We conclude that the α1 and α3 GlyR TM4 domains are orientated differently relative to their TM3 domains. This may underlie their differential ability to influence glycine efficacy.

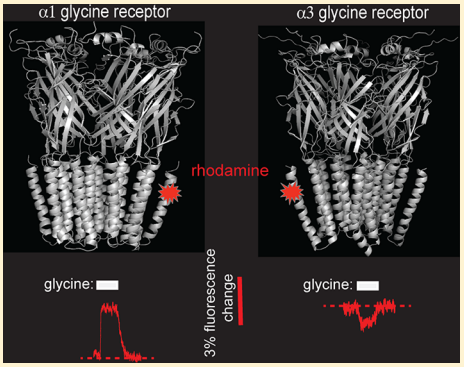

KEYWORDS: *Binding site, pLGIC, Cys-loop receptor, voltage clamp, fluorescence, mutagenesis,*

Pentameric ligand-gated ion channels (pLGICs) are a family of membrane proteins that mediate fast neurotransmission in the brain. Functional pLGICs comprise five homologous subunits arranged symmetrically around a central pore. The extracellular N-terminal domain is composed of 11 β-strands organized into a β-sheet sandwich with neurotransmitter-binding sites located at subunit interfaces. The transmembrane (TM) domain is composed of four membrane-spanning α-helices, termed TM1−TM4. A TM2 domain contributed by each of the five subunits lines the central pore. The TM2 domains are surrounded by the TM1, TM3, and TM4 domains that together provide a barrier between the hydrophilic pore and the hydrophobic membrane. The TM4 domain is largely surrounded by lipid and forms contacts with both TM1 and TM3. The TM4 extends beyond the other TM helices into the extracellular solution with its α-helical structure being maintained until the C-terminus.[1]

The glycine receptor (GlyR) is an anion-permeable pLGIC that mediates inhibitory neurotransmission in the spinal cord, retina, and brainstem.[2] A total of five GlyR subunits (α1−α4, β) are known, and most synaptic GlyRs comprise α1β heteromers. Although the distribution of α3 subunits is generally limited, α3-containing GlyRs are highly expressed in inhibitory synapses on spinal nociceptive neurons.[3] The α3 GlyR has thus emerged as a therapeutic target for analgesia, and indeed, drugs that specifically enhance α3 GlyR currents are effective in treating inflammatory and neuropathic pain.[4] Because residues lining the neurotransmitter-binding sites of the α1 and α3 GlyRs are highly conserved, it seems unlikely that this binding-site could be successfully targeted by subunit-specific modulators. It is therefore important to identify alternate drug-binding sites that may exhibit a greater structural diversity between these GlyR isoforms. One possible site, known as the intrasubunit alcohol-binding site, is formed by the outer regions of all four TM α-helices.[5]

Glycine exhibits a much higher efficacy for the α1 GlyR than for the α3 GlyR.[6] We recently employed a chimeric approach to show that their structurally divergent TM4 domains are responsible for a large part of this efficacy difference.[6] Because mutation of individual nonconserved TM4 residues had little effect on glycine efficacy, we concluded that the efficacy difference could not be attributed to specific molecular interactions but was more likely a distributed effect of all nonconserved TM4 residues. This prompted us to speculate that the TM4 domains of the α1 and α3 GlyRs must differ either in their secondary structures, membrane orientation, and/or molecular dynamic properties in either the closed and/or glycine-activated states. If so, then the intrasubunit alcohol binding site, to which the TM4 domain contributes, might be promising to investigate as a potential site for α3-specific modulators.

Here, we employed voltage-clamp fluorometry (VCF) to test the hypothesis that the TM4 domains of the α1 and α3 GlyRs interact differently relative to their respective TM3 domains in the closed and/or open states.

Received: October 10, 2012
Accepted: November 26, 2012
Published: November 26, 2012

RESULTS AND DISCUSSION

Relative to the α1 GlyR, the α3 GlyR contains two extra residues at the C-terminus (Figure 1A). Throughout the remainder of their TM4 domains, they share a 22/31 (= 71%) sequence identity and a 29/31 (= 94%) sequence homology. Full length homology structures of the α1 and α3 GlyRs were constructed using the *Caenorhabditis elegans* α1 glutamate-gated chloride channel (GluClR) crystal structure as a template.[1] The sequence alignment used to generate these models is shown in Figure S1 (Supporting Information). The predicted structure of the α1 GlyR TM4 is shown in Figure 1A. The backbone structure of the α3 GlyR TM4 domain was almost identical, and in our full length receptor structures the respective domains subtended a common angle relative to the remainder of the protein. A significant difference, however, was that the α3 TM4 domain was rotated around its long axis by around 30° relative to the α1 GlyR TM4 domain. This is illustrated in Figure 1B and C by showing the α1 R414 side chain in blue and the corresponding α3 R422 side chain in orange. In Figure 1C, we chose an Arg rotamer that maximized the angular difference. The relative positioning of TM3 and TM4 residues along their helical axes in our α1 GlyR model is supported by an electrophysiological study that provided evidence for a disulfide bond between A288C and Y410C in the α1 GlyR.[7]

We employed VCF to investigate whether the TM4 domains of α1 and α3 GlyRs are oriented differentially relative to their TM3 domains in the closed and/or open states. VCF reports changes in the quantum efficiency of rhodamine derivatives that occur in response to changes in the polarity of their microenvironment.[8,9] VCF involves introducing a cysteine into an otherwise cysteine-less receptor and covalently linking a thiosulfonate-tagged fluorophore to this introduced cysteine via a disulfide bond. By simultaneously recording current and fluorescence (ΔI and ΔF, respectively) responses, openings of the channel gate can be temporally correlated with conformational changes occurring in or around the labeled domain of interest.

As a first step, we individually mutated to cysteine all α1 GlyR TM4 residues from I409 to Q421, inclusive. After functionally expressing each mutant GlyR in *Xenopus* oocytes, we attempted to label each introduced cysteine in turn with MTSR and MTS-TAMRA (see Methods). The α1-I409C and α1-I410C GlyRs were not productively labeled by either compound, and the α1-K411C GlyR was labeled by MTSR only (see below). The other 10 residues (α1-I412C–α1-Q421C) were all productively labeled by both MTS-TAMRA and MTSR, although MTS-TAMRA was used for further experiments as it yielded a dramatically larger maximal fluorescence response (ΔF_{max}) at each labeled site. Given that disulfide bond formation between thiosulfonates and sulfhydryl groups requires a polar environment,[10] we inferred that the reactive residues face an aqueous environment. The locations of the 11 cysteine-substituted residues investigated in this study are shown in blue in Figure 1A.

Glycine dose–response relationships were quantitated for each cysteine mutant GlyR prior to labeling, with all averaged ΔI glycine EC_{50}, Hill coefficient (n_H), and ΔI_{max} values presented in Table 1. This analysis was repeated after covalent modification by either MTSR (α1-K411C) or MTS-TAMRA (α1-I412C–α1-R421C), with the averaged ΔI glycine EC_{50}, n_H, and ΔI_{max} values also presented in Table 1. All labeled mutants produced detectable ΔF values in response to glycine activation. Sample ΔI and ΔF dose–response relationships recorded from MTS-TAMRA-labeled α1-V413C, α1-R414C, α1-R415C, and α1-E416C GlyRs are shown in Figure 2 together with their averaged ΔI and ΔF concentration–response relationships. The averaged ΔF glycine EC_{50}, n_H, and ΔF_{max} values for these and all other tested α1 GlyR mutants are summarized in Table 1.

Figure S2 (Supporting Information) graphically illustrates several salient features of these results. The ΔI_{max} values (Figure S2A) and the ΔI and ΔF glycine EC_{50} values (Figure S2B) did not vary significantly for any tested mutant relative to any other mutant using one-way ANOVA and either Bonferroni or Dunnetts post hoc tests. Moreover, pairwise comparisons of the same parameters relative to the corresponding unmutated GlyR values using an unpaired t test revealed a similar result (Table 1). These results imply that mutagenesis and labeling did not significantly impair the function of any of the constructs investigated here. Figure S2B also shows that most of the mutants exhibited ΔF EC_{50} values that were around an order of magnitude higher than the corresponding ΔI EC_{50} values. The sole exception to this was the α1-R414C GlyR where the respective EC_{50} values were much closer in value (Figure S2B). Two points are worthy of note concerning the mean ΔF_{max} values as summarized in Figure S2C. First, the MTSR labeled α1-K411C GlyR exhibited an ΔF_{max} that was too small to permit quantitation of its glycine EC_{50} value. Second, the MTS-TAMRA labeled α1-R414C GlyR exhibited a ΔF_{max} that was opposite in sign to those of all the other tested mutants (see also Figure 2B). From all these results, we infer that the microenvironment of the

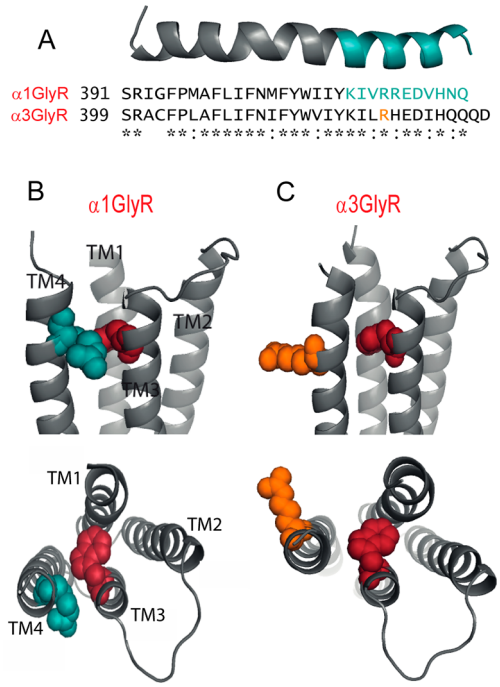

Figure 1. Comparison of TM4 domains in α1 and α3 GlyRs. (A) Sequence alignment of TM4 domains and C-terminal tails, together with a homology model of the α1 TM4 domain. Residues investigated in this study are colored blue in the model and in the primary sequence. (B) Structural model of the outer TM region of the α1 GlyR, viewed from within the membrane, with the W286 and R414 side chains colored red and blue, respectively. Lower panel shows a view from the synapse with extracellular domain removed. (C) Corresponding views of the α3 GlyR structure, with the W286 and R422 side chains colored red and orange, respectively. The position of R422 in the α3 primary sequence is shown in orange in (A).

dx.doi.org/10.1021/cn300177g | ACS Chem. Neurosci. 2013, 4, 248–254

Table 1. Properties of Agonist-Activated ΔI and ΔF Responses at Mutant α1 GlyRs[a]

construct	EC_{50} (μM)	n_H	ΔI_{max} (μA)	ΔF_{max} (%)	n
α1-WT unlabeled ΔI	17.9 ± 1.5	2.8 ± 0.1	4.8 ± 0.4		4
α1-WT labeled ΔI	17.1 ± 0.6	2.8 ± 0.2	4.9 ± 0.7		4
α1-WT labeled ΔF					**4**
α1-K411C unlabeled ΔI	45 ± 3^{aaa}	3.2 ± 0.5	4.5 ± 0.8		4
α1-K411C labeled ΔI	88 ± 6^{bb}	2.3 ± 0.3^{c}	3.3 ± 0.5		4
α1-K411C labeled ΔF				**−1.4 ± 0.2**	**4**
α1-I412C unlabeled ΔI	17.4 ± 3.7	2.0 ± 0.3	4.7 ± 0.4		4
α1-I412C labeled ΔI	7.7 ± 0.6^{c}	1.9 ± 0.4	2.2 ± 0.3		5
α1-I412C labeled ΔF	**153 ± 4^{ccc}**	**1.0 ± 0.1**		**−5.3 ± 0.5**	**5**
α1-V413C unlabeled ΔI	26.6 ± 4.8	1.9 ± 0.4	4.3 ± 0.4		5
α1-V413C labeled ΔI	8.4 ± 0.7^{bb}	2.1 ± 0.2	2.5 ± 0.1		6
α1-V413C labeled ΔF	**262 ± 44^{ccc}**	**2.1 ± 0.3**		**−27.0 ± 1.8**	**6**
α1-R414C unlabeled ΔI	24.3 ± 1.1^{b}	2.9 ± 0.1	2.4 ± 0.3		4
α1-R414C labeled ΔI	20.5 ± 2.9	2.6 ± 0.4	2.3 ± 0.3		6
α1-R414C labeled ΔF	**41 ± 7^{d}**	**1.5 ± 0.1^{d}**		**+3.1 ± 0.4**	**6**
α1-R415C unlabeled ΔI	11.5 ± 1.4^{b}	2.7 ± 0.3	3.1 ± 0.3		5
α1-R415C labeled ΔI	11.2 ± 0.6	2.6 ± 0.2	2.5 ± 0.2		6
α1-R415C labeled ΔF	**277 ± 23^{ccc}**	**1.5 ± 0.1^{cc}**		**−17.6 ± 1.6**	**6**
α1-E416C unlabeled ΔI	8.0 ± 1.0^{aa}	2.9 ± 0.1	2.7 ± 0.1		5
α1-E416C labeled ΔI	8.0 ± 0.8	2.3 ± 0.3	2.6 ± 0.2		5
α1-E416C labeled ΔF	**369 ± 28^{ccc}**	**1.1 ± 0.2^{d}**		**−7.9 ± 1.7**	**5**
α1-D417C unlabeled ΔI	10.1 ± 0.2^{b}	3.1 ± 0.2	3.1 ± 0.3		3
α1-D417C labeled ΔI	8.6 ± 0.4	2.3 ± 0.2	2.6 ± 0.1		5
α1-D417C labeled ΔF	**217 ± 19^{ccc}**	**2.1 ± 0.2^{d}**		**−11.3 ± 1.2**	**5**
α1-V418C unlabeled ΔI	13.3 ± 0.9	3.6 ± 0.7	3.2 ± 0.7		4
α1-V418C labeled ΔI	6.7 ± 0.8^{c}	2.2 ± 0.2^{c}	2.7 ± 0.1		5
α1-V418C labeled ΔF	**318 ± 35^{cc}**	**1.1 ± 0.1^{d}**		**−6.9 ± 0.3**	**5**
α1-H419C unlabeled ΔI	13.7 ± 1.3	3.6 ± 0.2	2.9 ± 0.2		4
α1-H419C labeled ΔI	14.9 ± 1.6	3.1 ± 0.2	2.7 ± 0.2		5
α1-H419C labeled ΔF	**311 ± 21^{ccc}**	**1.4 ± 0.1^{cc}**		**−9.3 ± 1.9**	**5**
α1-N420C unlabeled ΔI	14.5 ± 0.8	3.3 ± 0.1	2.9 ± 0.2		5
α1-N420C labeled ΔI	24.7 ± 4.4	2.1 ± 0.3^{bb}	3.1 ± 0.1		6
α1-N420C labeled ΔF	**288 ± 22^{ccc}**	**1.9 ± 0.1**		**−11.9 ± 1.1**	**6**
α1-Q421C unlabeled ΔI	14.8 ± 1.5	3.4 ± 0.6	3.5 ± 0.1		5
α1-Q421C labeled ΔI	26.7 ± 4.6	1.7 ± 0.3^{c}	3.0 ± 0.2		5
α1-Q421C labeled ΔF	**329 ± 13^{ccc}**	**1.8 ± 0.1**		**−11.7 ± 0.8**	**5**
α1-W286F-V413C unlabeled ΔI	475 ± 14^{aaa}	3.1 ± 0.2	5.7 ± 0.4		3
α1-W286F−V413C labeled ΔI	190 ± 56^{bb}	2.2 ± 0.1^{c}	5.7 ± 0.3		4
α1-W286F-V413C labeled ΔF				**−2.5 ± 0.4**	**4**
α1-W286F-R414C unlabeled ΔI	792 ± 20^{aaa}	3.0 ± 0.2	4.7 ± 0.4		5
α1-W286F-R414C labeled ΔI	182 ± 34^{bbb}	2.0 ± 0.2^{c}	3.7 ± 0.4		5
α1-W286F-R414C labeled ΔF				**−1.8 ± 0.3**	**5**
α1-W286F-R415C unlabeled ΔI	602 ± 89^{aaa}	3.2 ± 0.1	3.9 ± 0.4		3
α1-W286F-R415C labeled ΔI	213 ± 67^{bbb}	2.1 ± 0.1^{bb}	3.8 ± 0.2		5
α1-W286F-R415C labeled ΔF				**−2.2 ± 1.2**	**5**
α1-W286F-E416C unlabeled ΔI	579 ± 69^{aaa}	3.2 ± 0.4	3.3 ± 0.6		3
α1-W286F-E416C labeled ΔI	199 ± 19^{bb}	2.0 ± 0.2^{c}	3.2 ± 0.2		4
α1-W286F-E416C labeled ΔF				**−1.8 ± 0.4**	**4**

[a]Electrophysiological and fluorescence data are shown in normal and bold type, respectively. [b]Significant difference to electrophysiological properties of unlabeled α1-WT GlyRs (unpaired Student's t test, $^{a}p < 0.05$, $^{aa}p < 0.01$, $^{aaa}p < 0.001$). [c]Significant difference to electrophysiological properties before labeling in the same mutant GlyR (unpaired Student's t test, $^{b}p < 0.05$, $^{bb}p < 0.01$, $^{bbb}p < 0.001$). [d]Significant difference of fluorescence properties to electrophysiological properties after labeling in the same mutant GlyR (paired Student's t test, $^{c}p < 0.05$,$^{cc}p < 0.01$, $^{ccc}p < 0.001$).

label attached to the α1-R414C GlyR differs from that of the labels attached to the other residues. We thus hypothesize that the label attached to α1-R414C exhibits a glycine-dependent interaction with another chemical group.

Our α1 GlyR model predicts that R414 faces toward W286 in TM3 (Figure 1B). We therefore hypothesized that the rhodamine derivative attached to R414C interacts with W286 in a glycine-dependent manner. As our model of the α3 GlyR predicts that α3-R422 (which corresponds to α1-R414) is orientated differently relative to W286 (Figure 1C), we predict that the rhodamine derivative attached to α3-R422 exhibits a differential interaction with W286. To test these predictions, we investigated the effects of the W286F mutation on the glycine-induced ΔF responses of rhodamine derivatives attached

dx.doi.org/10.1021/cn300177g | ACS Chem. Neurosci. 2013, 4, 248−254

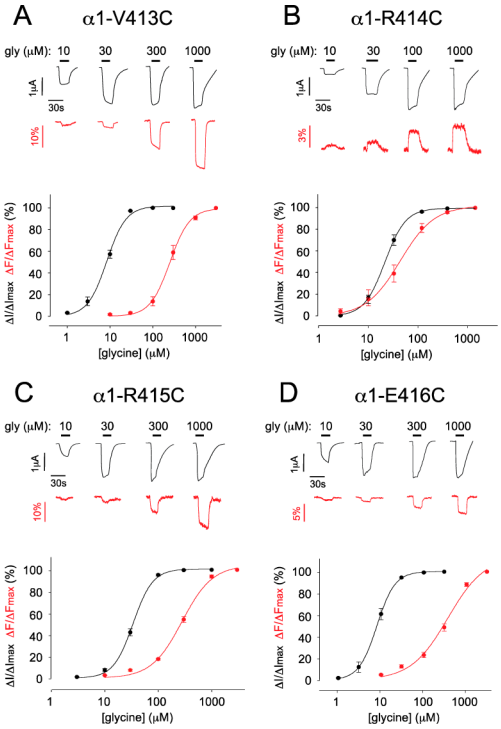

Figure 2. Sample ΔI and ΔF recordings and their averaged dose–response relationships from MTS-TAMRA-labeled α1-V413C GlyRs (A), α1-R414C GlyRs (B), α1-R415C GlyRs (C), and α1-E416C GlyRs (D). In this and subsequent figures, glycine-induced ΔI and ΔI responses are shown in black and red, respectively, and glycine applications are indicated by black bars. Mean ΔI and ΔF glycine EC_{50}, n_H, ΔI_{max}, and ΔF_{max} values of best fit to individual dose–response relations are presented in Table 1.

individually to V413C, R414C, R415C, or E416C in the α1 GlyR and L421C, R422C, H423C, or E424C in the α3 GlyR.

Glycine dose–response relationships were quantitated for the double mutant α1-W286F-V413C GlyR, α1-W286F-R414C GlyR, α1-W286F-R415C GlyR, and α1-W286F-E416C GlyRs before and after labeling with MTS-TAMRA, with all averaged ΔI glycine EC_{50}, n_H, and ΔI_{max} values presented in Table 1. The W286F mutation dramatically increased the glycine EC_{50} values of all four constructs, although MTS-TAMRA labeling tended to reverse this trend. The W286F mutation also produced a dramatic, uniform reduction in the ΔF_{max} values of all four labeled double mutant α1 GlyRs (Figure 3A, B). However, the sign of glycine-induced ΔF_{max} was not changed in the α1-W286F-V413C GlyR, the α1-W286F-R415C GlyR, and the α1-W286F-E416C GlyR. Together these results imply a nonspecific, indirect effect of W286F on receptor gating efficacy and on the propensity of labels attached to TM4 residues to experience an altered microenvironment between the unliganded and glycine-activated states. However, in contrast to these results, the sign of the glycine-induced ΔF_{max} at the labeled α1-W286F-R414C GlyR was reversed relative to the α1-R414C GlyR (Table 1, Figure 3B). This indicates that the glycine-induced micro-environmental change at the label attached to this R414C was altered by W286F. This in turn provides strong support for a specific interaction between W286 and the label attached to R414C, as predicted by our model.

A similar experimental approach was applied to the α3 GlyR. Glycine dose–response relationships were quantitated for the single mutant α3-L421C, α3-R422C, α3-H423C and α3-E424C GlyRs both before and after labeling with MTS-TAMRA, and all averaged ΔI glycine EC_{50}, n_H and ΔI_{max} values are presented in Table 2. As with the corresponding α1 GlyR mutations, these mutations had little effect on ΔI_{max} or glycine EC_{50} values. Surprisingly, glycine-induced ΔF_{max} responses were invariably much smaller than those observed at the corresponding α1 GlyR mutants, and for this reason the ΔF glycine EC_{50} values could not be quantitated (Table 2, Figure 3C). Introduction of the W286F

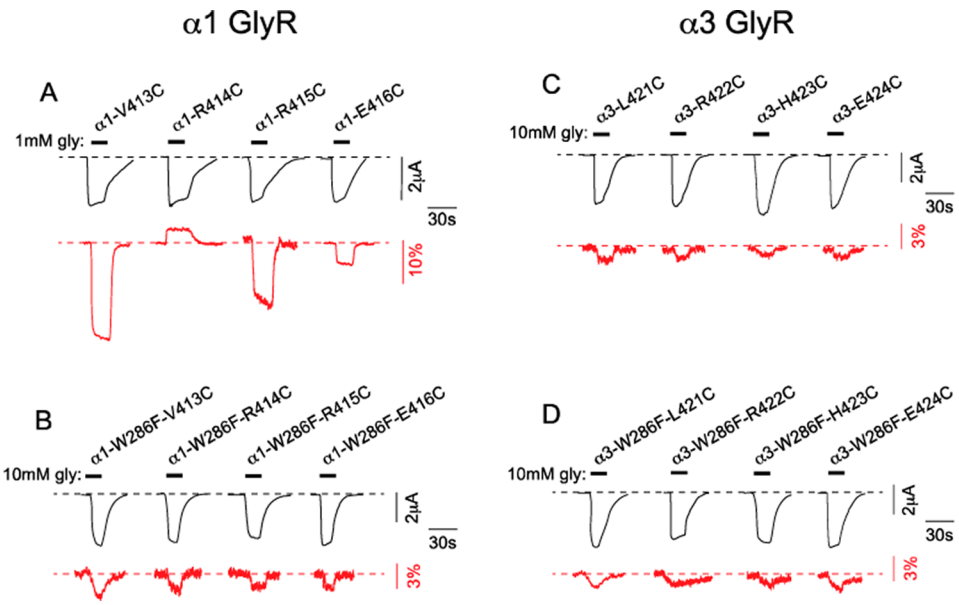

Figure 3. Effect of the W286F mutation on the functional properties of MTS-TAMRA-labeled mutant α1 and α3 GlyRs. (A) Examples of ΔI_{max} and ΔF_{max} responses induced by saturating glycine in the indicated single mutant α1 GlyRs. The four traces are reproduced from Figure 2. (B) Examples of ΔI_{max} and ΔF_{max} responses induced by saturating glycine in double mutant α1 GlyRs. (C) Examples of ΔI_{max} and ΔF_{max} responses induced by saturating glycine in the corresponding single mutant α3 GlyRs. (D) Examples of ΔI_{max} and ΔF_{max} responses induced by saturating glycine in the corresponding double mutant α3 GlyRs. All averaged values are given in Tables 1 and 2.

dx.doi.org/10.1021/cn300177g | ACS Chem. Neurosci. 2013, 4, 248–254

Table 2. Properties of Agonist-Activated ΔI and ΔF Responses at Mutant α3 GlyRs[a]

construct	EC_{50} (μM)	n_H	I_{max} (μA)	ΔF_{max} (%)	n
α3-WT unlabeled ΔI	74 ± 2	2.9 ± 0.2	5.4 ± 0.6		6
α3-WT labeled ΔI	71 ± 2	2.9 ± 0.2	5.6 ± 0.5		6
α3-WT labeled ΔF					**6**
α3-L421C unlabeled ΔI	27.1 ± 0.3^{aaa}	2.5 ± 0.1	4.1 ± 0.2		3
α3-L421C labeled ΔI	31 ± 1	2.6 ± 0.2	4.6 ± 0.4		4
α3-L421C labeled ΔF				**−1.8 ± 0.1**	**4**
α3-R422C unlabeled ΔI	35 ± 2^{aaa}	2.6 ± 0.3	3.7 ± 0.3		3
α3-R422C labeled ΔI	23.9 ± 0.4	3.8 ± 0.2^{c}	4.9 ± 0.6		5
α3-R422C labeled ΔF				**−1.2 ± 0.1**	**5**
α3-H423C unlabeled ΔI	36 ± 1^{aaa}	3.0 ± 0.2	4.9 ± 0.3		3
α3-H423C labeled ΔI	36 ± 2	3.6 ± 0.6	5.2 ± 0.4		4
α3-H423C labeled ΔF				**−0.9 ± 0.1**	**4**
α3-E424C unlabeled ΔI	52 ± 2^{aa}	2.8 ± 0.1	4.3 ± 0.5		4
α3-E424C labeled ΔI	28.2 ± 0.5^{c}	2.8 ± 0.2	4.9 ± 0.7		5
α3-E424C labeled ΔF				**−0.9 ± 0.2**	**5**
α3-W286F-L421C unlabeled ΔI	898 ± 59^{aaa}	3.0 ± 0.4	3.9 ± 0.3		3
α3-W286F-L421C labeled ΔI	165 ± 36^{bbb}	2.0 ± 0.3^{c}	2.5 ± 0.5		3
α3-W286F-L421C labeled ΔF				**−2.1 ± 0.3**	**3**
α3-W286F-R422C unlabeled ΔI	934 ± 70^{aaa}	3.3 ± 0.1	2.9 ± 0.2		3
α3-W286F-R422C labeled ΔI	248 ± 44^{bbb}	2.4 ± 0.4^{c}	2.8 ± 0.3		4
α3-W286F-R422C labeled ΔF				**−1.3 ± 0.2**	**4**
α3-W286F−H423C unlabeled ΔI	742 ± 62^{aaa}	3.4 ± 0.4	3.3 ± 0.3		3
α3-W286F−H423C labeled ΔI	277 ± 65^{bb}	1.8 ± 0.3^{bb}	2.7 ± 0.2		5
α3-W286F-H423C labeled ΔF				**−1.5 ± 0.3**	**5**
α3-W286F-E424C unlabeled ΔI	798 ± 82^{aaa}	3.0 ± 0.4	3.8 ± 0.5		3
α3-W286F-E424C labeled ΔI	236 ± 35^{bbb}	1.8 ± 0.3^{bb}	2.8 ± 0.3		3
α3-W286F-E424C labeled ΔF				**−1.8 ± 0.4**	**3**

[a]Electrophysiological and fluorescence data are shown in normal and bold type, respectively. [b]Significant difference to electrophysiological properties of unlabeled α1-WT GlyRs (unpaired Student's t test, $^{a}p < 0.05$, $^{aa}p < 0.01$, $^{aaa}p < 0.001$). [c]Significant difference to electrophysiological properties before labeling in the same mutant GlyR (paired Student's t test, $^{b}p < 0.05$, $^{bb}p < 0.01$, $^{bbb}p < 0.001$).

mutation produced a dramatic increase in ΔI glycine EC_{50} without significantly affecting the ΔI_{max} values (Table 2, Figure 3D). MTS-TAMRA labeling significantly reduced the ΔI glycine EC_{50} values at all four mutant receptors (Table 2). All of these effects were similar to those observed at the α1 GlyR, implying a nonspecific effect of the W286F mutation on the gating efficacy of both GlyRs. However, for all four double mutant α3 GlyRs, neither the sign nor the magnitude of glycine-induced ΔF_{max} was altered by the W286F mutation (Table 2, Figure 3D). We thus infer that the label attached to R422C in the α3 GlyR exhibits a different interaction with W286F than the one attached to R414C in the α1 GlyR. This provides strong evidence for a differential orientation of the α1 and α3 TM4 domains relative to their TM3 domains during glycine-activation.

There is currently little information as to how TM4 domains contribute to channel activation. In the muscle nicotinic receptor, the TM4 domain moves as a unit approximately midway through the gating reaction.[11] Molecular dynamics simulations concur with the idea of TM4 moving as a rigid α-helix, but with relatively small amplitude movements.[12] Electrophysiological studies on a variety of pLGICs have shown that mutations to TM4 residues strongly influence gating efficacy in a manner that suggests altered interactions with the surrounding lipid environment.[6,13−16] Indeed, biochemical investigations have shown that TM4 orientation and movement is altered by the lipid environment[17] and that this in turn can potently modulate channel gating efficacy.[18] However, there is as yet no information as to whether structurally conserved TM4 domains in homologous pLGIC subunits may be oriented differently with respect to the remainder of the protein. This is the issue that the present study sought to address.

Before interpreting our data, it is necessary to consider the limitations of VCF for interpreting conformational changes in ligand-gated ion channels. Briefly, a ligand-induced ΔF implies that the microenvironment of an attached fluorophore has been altered via a direct fluorophore−ligand interaction, a ligand-induced conformational change associated with channel opening, and/or a ligand-induced conformational change associated with a mechanism (e.g., desensitization) unrelated to channel opening. Although we can eliminate direct fluorophore−ligand interactions on the grounds that TM4 is distant from the glycine-binding site, we cannot discriminate between the other two possibilities. However, as the ΔF EC_{50} was an order of magnitude higher than the ΔI EC_{50} at most mutants (Figure S2B, Supporting Information), we infer that the movements we detected in TM4 reflect either high levels of binding site occupancy or entry into a desensitized state. In either case, it is possible that the movements reported here may not essential to weakly activate the channels.

In the α1 GlyR, labels attached to 10 of the 11 TM4 sites responded to glycine in a remarkably similar manner, with negative ΔF's and large offsets between ΔI and ΔF glycine EC_{50}'s (Figure S2B). It is not easy to explain the uniformity of these responses. We infer these ΔF's occurred in response to a generically altered lipid/water environment. The alternative possibility, that the ΔFs were due to state-dependent differences in molecular interactions with neighboring receptor domains, is unlikely given that all ΔFs varied in the same direction. For

dx.doi.org/10.1021/cn300177g | ACS Chem. Neurosci. 2013, 4, 248−254

example, in this scenario, labels attached to sites facing away from TM3 should have produced no ΔF at all. The sole exception to this rule was the response of the label attached to R414C. The reversed hydrophobicity change at this site implies a different chemical origin from those that occurred at the other labeled sites. The similarity of the ΔI and ΔF glycine EC_{50} values implies the label may have sensed a conformational change in the TM3 that was associated with activation. Mutagenesis of W286 confirmed this interaction.

In contrast, W286F did not affect the sign or magnitude of the ΔF at the labeled R422C mutant α3 GlyR. Thus, labels attached to homologous residues in α1 and α3 GlyRs do not sense the same microenvironmental change during activation. This strongly suggests that the respective TM4 domains exhibit different secondary structures, membrane orientations, or molecular dynamic properties in either the closed and/or glycine-activated states. As our molecular modeling predicts that the respective TM4 domains have modestly different orientations relative to TM3, it provides support for this conclusion. However, as our models are based on a crystal structure, they may not accurately reflect the orientations of the TM4 domains under physiological lipid conditions. It is also important to consider that we excised the large intracellular TM3−4 domains to generate our models. As these domains differ in length between α1 and α3 GlyRs, their presence may influence TM4 orientation and molecular dynamic properties. Thus, we consider the models may not be sufficiently precise to accurately interpret our results.

In summary, we conclude that the TM4 domains of the α1 and α3 GlyRs differ either in their secondary structures, membrane orientations, or molecular dynamic properties in either the closed and/or glycine-activated states. This may explain their capacity to differentially influence glycine efficacy. It also suggests that the intrasubunit alcohol binding site to which each TM4 domain contributes might be promising to investigate as a potential binding site for α3-specific modulators.

METHODS

Molecular Biology. Plasmid DNAs for the human α1 and rat α3 GlyR subunits were each subcloned into the pGEMHE vector. All constructs employed in this study were made on the C41A background to eliminate the only uncross-linked extracelular cysteine. QuickChange (Stratagene, La Jolla, CA) was used to generate all mutants used in this study. Automated sequencing of the entire coding sequence was used to confirm the successful incorporation of mutations. Capped mRNA for oocyte injection was generated using mMessage mMachine (Ambion, Austin, TX).

Oocyte Preparation, Injection, and Labeling. Oocytes from female *Xenopus laevis* (*Xenopus* Express, France) were prepared as previously described[19] and injected with 10 ng of mRNA. The oocytes were then incubated at 18 °C for 3−5 days in ND96 solution containing 96 mM NaCl, 2 mM KCl, 1 mM $MgCl_2$, 1.8 mM $CaCl_2$, 5 mM HEPES, 0.6 mM theophylline, 2.5 mM pyruvic acid, 50 μg/mL gentamycin, pH 7.4.

Fluorophore Labeling. Rhodamine methanethiosulfonate (MTSR) and 2-((5(6)-tetramethylrhodamine)carboxylamino)ethyl methanethiosulfonate (MTS-TAMRA), both from Toronto Research Chemicals (North York, ON), were dissolved in dimethyl sulfoxide and stored at −20 °C. On the day of recording, oocytes were incubated for 30 s in 10 μM MTSR or MTS-TAMRA dissolved in ice-cold ND96. Oocytes were then thoroughly washed and stored in ND96 for up to 6 h on ice before recording. As unmutated α1 and α3 GlyRs never exhibited a glycine-induced fluorescence change (ΔF) or a change in electrophysiological properties following fluorophore incubation[19] (Table 1), we can rule out nonspecific labeling.

VCF and Data Analysis. Oocytes were placed in a recording chamber on an inverted microscope.[20] The microscope was equipped with a high-Q tetramethylrhodamine isothiocyanate filter set (Chroma Technology, Rockingham, VT), a Plan Fluor 40× objective lens (Nikon Instruments, Kawasaki, Japan), and a Hamamatsu H7360-03 photomultiplier (Hamamatsu Photonics, Hamamatsu City, Japan) coupled to a PMT400R photomultiplier subsystem (Ionoptix, Milton, MA). A 150 W halogen lamp was used as light source. Cells were maintained at −40 mV by conventional two-electrode voltage-clamp and currents were recorded with a Gene Clamp 500B amplifier (Axon Instruments, Union City, CA). Current and fluorescence traces were acquired at 200 Hz via a Digidata 1322A interface using Clampex 9.2 software (Axon Instruments, Union City, CA). For analysis and display, fluorescence signals were digitally filtered at 1−2 Hz with an eight-pole Bessel filter. Results are expressed as mean ± SEM of three or more independent experiments. The Hill equation was used to calculate the EC_{50} and n_H values for glycine activation. All curves were fitted using a nonlinear least-squares algorithm (Sigmaplot 9.0, Jandel Scientific, San Rafael, CA).

Molecular Modeling. Full length human α1 and rat α3 GlyR structures were modeled on the *C. elegans* α GluClR crystal structure (PDB code: 3RIF).[1] The alignment between GluClR and the GlyR subunits was optimized using CLUSTAL W. Based on alignment, the GlyR sequences were edited to excise the large intracellular TM3−4 domain. Modeler v9.10 was then used to generate the tertiary structure models. The variable target function method was used initially to generate 50 randomized models.[21] The quality of these models were compared in terms of various statistically derived structure quality assessment scales that included Ramachandran Plot, Errat Score, Z-Score, and initial packing quality.[22−24] Structures with the highest Z-scores were selected for energy minimizations using Gromacs. Unfavorable contacts in each structure were relieved by two cycles (5000 steps each) of steepest distance and conjugate gradient minimizations.[25] To further validate the structure, the standard ligands glycine and strychnine were docked using FlexX.[26] The pose output limit was set to 20 for each run for extensive conformational sampling. For both the α1 and α3 GlyRs, the docked orientations were found to be identical to the binding orientations as shown in previous studies.[27,28]

ASSOCIATED CONTENT

Supporting Information

Additional figures as described in the text. This material is available free of charge via the Internet at http://pubs.acs.org.

AUTHOR INFORMATION

Corresponding Author

*Telephone: (+617) 33466375. Fax: (+617) 33466301. E-mail: j.lynch@uq.edu.au.

Author Contributions

Participated in research design: H.L. and J.W.L. Conducted experiments and performed data analysis: H.L. and S.T. Wrote manuscript: H.L., S.T., and J.W.L.

Funding

Funding for this research was received from the Australian Research Council and the National Health and Medical Research Council of Australia.

Notes

The authors declare no competing financial interest.

ABBREVIATIONS

ΔF, change in fluorescence; ΔF_{max}, maximum change in fluorescence; ΔI, change in current; ΔI_{max}, maximum change in current; GluClR, glutamate-gated chloride channel receptor; GlyR, glycine receptor; MTSR, rhodamine methanethiosulfonate; MTS-TAMRA, 2-((5(6)-tetramethylrhodamine)carboxylamino)ethyl methanethiosulfonate; pLGIC, pentameric

ligand-gated ion channel; TM, transmembrane; VCF, voltage-clamp fluorometry

REFERENCES

(1) Hibbs, R. E., and Gouaux, E. (2011) Principles of activation and permeation in an anion-selective Cys-loop receptor. *Nature 474*, 54−60.

(2) Lynch, J. W. (2004) Molecular structure and function of the glycine receptor chloride channel. *Physiol. Rev. 84*, 1051−1095.

(3) Harvey, R. J., Depner, U. B., Wassle, H., Ahmadi, S., Heindl, C., Reinold, H., Smart, T. G., Harvey, K., Schutz, B., Abo-Salem, O. M., Zimmer, A., Poisbeau, P., Welzl, H., Wolfer, D. P., Betz, H., Zeilhofer, H. U., and Muller, U. (2004) GlyR alpha3: an essential target for spinal PGE2-mediated inflammatory pain sensitization. *Science 304*, 884−887.

(4) Xiong, W., Cui, T., Cheng, K., Yang, F., Chen, S. R., Willenbring, D., Guan, Y., Pan, H. L., Ren, K., Xu, Y., and Zhang, L. (2012) Cannabinoids suppress inflammatory and neuropathic pain by targeting alpha3 glycine receptors. *J. Exp. Med. 209*, 1121−1134.

(5) Howard, R. J., Murail, S., Ondricek, K. E., Corringer, P. J., Lindahl, E., Trudell, J. R., and Harris, R. A. (2011) Structural basis for alcohol modulation of a pentameric ligand-gated ion channel. *Proc. Natl. Acad. Sci. U.S.A. 108*, 12149−12154.

(6) Chen, X., Webb, T. I., and Lynch, J. W. (2009) The M4 transmembrane segment contributes to agonist efficacy differences between alpha1 and alpha3 glycine receptors. *Mol. Membr. Biol. 26*, 321−332.

(7) McCracken, L. M., McCracken, M. L., Gong, D. H., Trudell, J. R., and Harris, R. A. (2010) Linking of Glycine Receptor Transmembrane Segments Three and Four Allows Assignment of Intrasubunit-Facing Residues. *ACS Chem. Neurosci. 1*, 482−494.

(8) Gandhi, C. S., and Isacoff, E. Y. (2005) Shedding light on membrane proteins. *Trends Neurosci. 28*, 472−479.

(9) Pless, S. A., and Lynch, J. W. (2008) Illuminating the structure and function of Cys-loop receptors. *Clin. Exp. Pharmacol. Physiol. 35*, 1137−1142.

(10) Karlin, A., and Akabas, M. H. (1998) Substituted-cysteine accessibility method. *Methods Enzymol. 293*, 123−145.

(11) Mitra, A., Bailey, T. D., and Auerbach, A. L. (2004) Structural dynamics of the M4 transmembrane segment during acetylcholine receptor gating. *Structure 12*, 1909−1918.

(12) Cheng, X., Ivanov, I., Wang, H., Sine, S. M., and McCammon, J. A. (2007) Nanosecond-timescale conformational dynamics of the human alpha7 nicotinic acetylcholine receptor. *Biophys. J. 93*, 2622−2634.

(13) Li, L., Lee, Y. H., Pappone, P., Palma, A., and McNamee, M. G. (1992) Site-specific mutations of nicotinic acetylcholine receptor at the lipid-protein interface dramatically alter ion channel gating. *Biophys. J. 62*, 61−63.

(14) Lobo, I. A., Trudell, J. R., and Harris, R. A. (2006) Accessibility to residues in transmembrane segment four of the glycine receptor. *Neuropharmacology 50*, 174−181.

(15) Jenkins, A., Andreasen, A., Trudell, J. R., and Harrison, N. L. (2002) Tryptophan scanning mutagenesis in TM4 of the GABA(A) receptor alpha1 subunit: implications for modulation by inhaled anesthetics and ion channel structure. *Neuropharmacology 43*, 669−678.

(16) Lee, Y. H., Li, L., Lasalde, J., Rojas, L., McNamee, M., Ortiz-Miranda, S. I., and Pappone, P. (1994) Mutations in the M4 domain of Torpedo californica acetylcholine receptor dramatically alter ion channel function. *Biophys. J. 66*, 646−653.

(17) Barrantes, F. J. (2003) Modulation of nicotinic acetylcholine receptor function through the outer and middle rings of transmembrane domains. *Curr. Opin. Drug Discovery Dev. 6*, 620−632.

(18) daCosta, C. J., and Baenziger, J. E. (2009) A lipid-dependent uncoupled conformation of the acetylcholine receptor. *J. Biol. Chem. 284*, 17819−17825.

(19) Pless, S. A., Dibas, M. I., Lester, H. A., and Lynch, J. W. (2007) Conformational variability of the glycine receptor M2 domain in response to activation by different agonists. *J. Biol. Chem. 282*, 36057−36067.

(20) Dahan, D. S., Dibas, M. I., Petersson, E. J., Auyeung, V. C., Chanda, B., Bezanilla, F., Dougherty, D. A., and Lester, H. A. (2004) A fluorophore attached to nicotinic acetylcholine receptor beta M2 detects productive binding of agonist to the alpha delta site. *Proc. Natl. Acad. Sci. U.S.A. 101*, 10195−10200.

(21) Sali, A., Potterton, L., Yuan, F., van Vlijmen, H., and Karplus, M. (1995) Evaluation of comparative protein modeling by MODELLER. *Proteins 23*, 318−326.

(22) Colovos, C., and Yeates, T. O. (1993) Verification of protein structures: patterns of nonbonded atomic interactions. *Protein Sci. 2*, 1511−1519.

(23) Laskowski, R. A., Rullmannn, J. A., MacArthur, M. W., Kaptein, R., and Thornton, J. M. (1996) AQUA and PROCHECK-NMR: programs for checking the quality of protein structures solved by NMR. *J. Biomol. NMR 8*, 477−486.

(24) Wiederstein, M., and Sippl, M. J. (2007) ProSA-web: interactive web service for the recognition of errors in three-dimensional structures of proteins. *Nucleic Acids Res. 35*, W407−410.

(25) Van Der Spoel, D., Lindahl, E., Hess, B., Groenhof, G., Mark, A. E., and Berendsen, H. J. (2005) GROMACS: fast, flexible, and free. *J. Comput. Chem. 26*, 1701−1718.

(26) Rarey, M., Kramer, B., Lengauer, T., and Klebe, G. (1996) A fast flexible docking method using an incremental construction algorithm. *J. Mol. Biol. 261*, 470−489.

(27) Grudzinska, J., Schemm, R., Haeger, S., Nicke, A., Schmalzing, G., Betz, H., and Laube, B. (2005) The [beta] Subunit Determines the Ligand Binding Properties of Synaptic Glycine Receptors. *Neuron 45*, 727−739.

(28) Pless, S. A., Millen, K. S., Hanek, A. P., Lynch, J. W., Lester, H. A., Lummis, S. C., and Dougherty, D. A. (2008) A cation-pi interaction in the binding site of the glycine receptor is mediated by a phenylalanine residue. *J. Neurosci. 28*, 10937−10942.